

**Cite this article as:** Laixia Yang, Longbo Zhang, Qidong Xie, et al. Effects of the addition of CNTs on microstructure, mechanics and thermal conductivity of pure copper in laser powder bed melting.

ARTICLE

DOI: 10.12442/j.issn.1002-185X.20240754

# Effects of the addition of CNTs on microstructure, mechanics and thermal conductivity of pure copper in laser powder bed melting

Laixia Yang<sup>1</sup>, Longbo Zhang<sup>1</sup>, Qidong Xie<sup>2</sup>, Yanze Zhang<sup>1</sup>, Mengjia Yang<sup>1</sup>, Feng Mao<sup>3</sup>, Zhen Chen<sup>2</sup>

<sup>1</sup> School of Mechanical Engineering, Xi'an University of Science and Technology, Xi'an 710054, China; <sup>2</sup> School of Mechanical Engineering, Xi'an Jiaotong University, Xi'an 710049, China; <sup>3</sup> Longmen laboratory, Henan 471000, China

**Abstract:** The laser powder bed fusion (L-PBF) process for manufacturing copper typically exhibits poor strength-ductility coordination; the addition of enhancers is usually an effective way to improve it. However, there is relatively limited research on Cu composites. To explore the impact of enhancements on Cu, we used a Cu-CNTs mixed powder as the base and applied the L-PBF technology to produce a Cu-CNTs composite. We studied its forming performance, microstructure, and mechanical properties, as well as its conductive and thermal properties. The resulting composite has a high relative density of consolidated Cu-CNTs material. The addition of CNTs results in non-uniform microstructure with equiaxed grains at the edges of the melt pool and columnar grains at the center. Compared to pure copper, the overall mechanical properties of the composite are improved (tensile strength increased by 52.8%, elongation increased by 115.9%), and the electrical and thermal properties are also enhanced (thermal conductivity increased by 10.8%, electrical conductivity increased by 12.7%). The results indicate that the addition of CNTs can increase the tensile strength and elongation, as well as the electrical and thermal properties of copper. Therefore, this material provides an efficient pathway for designing more efficient heat sink structures.

**Key words:** laser powder bed melting; Cu-CNTs composites; Mechanical property; thermal conductivity

Pure copper is an important material with high electrical conductivity (International Annealed copper Standard [IACS] 102%) and 400 W/(m·K) thermal conductivity, widely used in heat transfer and electromagnetic fields. However, current traditional manufacturing techniques are unable to produce fine parts with complex geometric structures. As a result, metal additive manufacturing processes, especially L-PBF, have attracted attention due to their ability to manufacture geometrically complex parts from powder materials<sup>[1]</sup>. Combined with the ability to manufacture geometrically complex parts using L-PBF and the high thermal conductivity of pure copper, parts with higher heat transfer efficiency can be manufactured<sup>[2]</sup>.

However, due to the high laser reflectivity of copper to infrared radiation (especially at 1060-1080 nm, which corresponds to the near-infrared radiation of the most commonly used lasers in L-PBF) and very high thermal conductivity (the small heat absorbed by the instantaneous dissipation)<sup>[3]</sup>, the strength and density of the prepared samples generally cannot meet the requirements of use.

Currently, an effective method is to add other strengthening elements to the copper matrix material to enhance the matrix's strength. Using this approach, many researchers prefer pre-alloyed copper powder, which has slightly lower optical reflectivity than pure copper. This enables the production of

Received date:

Foundation item: National Key Research and Development Program of China (No.2023YFB4606400), the Longmen laboratory frontier exploration topics (No.LMQYTSKT003)

Corresponding author: Zhen Chen, Ph.D., Associate Professor, School of Mechanical Engineering, Xi'an Jiaotong University, Xi'an 710049, P.R. China, E-mail: [chenzhen2025@xjtu.edu.cn](mailto:chenzhen2025@xjtu.edu.cn)

Copyright © 2019, Northwest Institute for Nonferrous Metal Research. Published by Science Press. All rights reserved.

dense parts from alloys such as Cu-Cr<sup>[4]</sup>, Cu-Cr-Zr<sup>[5]</sup>, Cu-Sn<sup>[6]</sup>, and Cu-Zn<sup>[7]</sup> alloys. However, compared to pure copper parts in the built state, these materials' samples exhibit significantly improved density and much higher tensile strength. However, the addition of other metal elements with lower thermal conductivity in the samples seriously hinders the transmission of phonons and electrons, resulting in much lower thermal and electrical conductivity compared to pure copper samples<sup>[8]</sup>. Currently, nano-particle-reinforced metal matrix composites have proven to be one of the promising materials to address this need<sup>[9]</sup>. Adding nanomaterials with higher laser absorption and electrical conductivity to copper powder particles and using L-PBF technology to prepare composites with high strength, high thermal conductivity, and electrical conductivity has become a new trend. Therefore, this study utilizes nanoscale carbon nanotubes wrapped on the surface of pure copper powder to prepare samples with enhanced laser absorption, strength, and electrical and thermal conductivity. Although the idea of coating copper powder with carbon nanotubes was previously proposed<sup>[10]</sup>, the L-PBF behavior and resulting mechanical and thermal conductivity have not been reported.

Consequently, this study proposes an alternative method involving mixing carbon nanotubes with copper powder particles to enhance the powder's light absorption and L-PBF behavior. Subsequently, the effects of carbon nanotubes on the formability, microstructure, mechanical properties, electrical conductivity, and thermal conductivity of the composites were evaluated.

## 1 Experiment

The gas atomized copper powder (99.96% purity, D50:37.87 $\mu$ m, Asia New Materials Co., LTD., China) and multi-walled carbon nanotubes (diameter 4-6nm, Jiangsu Xianfeng Nanomaterials Technology Co., LTD., China) were used as the initial materials. 0.3wt% CNTs were dispersed in anhydrous ethanol. The beaker containing the solution was placed in a water bath, along with the probe of an ultrasonic homogenizer. The solution was uniformly shaken by the ultrasonic homogenizer until the CNTs were evenly dispersed. Pure copper powder was added to the solution, and the mixed solution was evenly mixed in a vacuum homogenizer. The equipment used was the ZYMC-200V vacuum homogenizer. Powder mixing was carried out in three variable speed rotation modes: 1500 rpm for 20s, 2500rpm for 30s, 1000rpm for 15s. The particle size distribution of the Cu-0.3wt% CNTs mixed powder was measured by an LS-909 laser diffraction particle size analyzer (Omicron, China) in wet mode. Before the L-PBF process, the powder was dried in a vacuum drying oven for 10 hours at 120°C. Vacuum drying can remove water from the powder, enhance its fluidity, and effectively prevent the oxidation of the Cu-0.3wt% CNTs mixed powder during the L-PBF process.

The optical reflectance of the powder was measured at room temperature using a UV-visible near-infrared spectrophotometer (model numbers: Shimadzu UV3600, Agilent CARY 300, and PE lambda 750S). Measurements were made in total reflection mode, using a spectrum of 100% reflectance as the reference material. Using the formula "Light absorption (%) = 100 - light reflection (%)", the light absorption was calculated from the reflectance measurement results.

Selective laser melting (L-PBF) was performed on a machine developed by the Department of Mechanical Engineering of Xi'an Jiaotong University. Throughout the construction process, oxygen levels were maintained below 100ppm by filling the build chamber with protective argon. The fiber laser wavelength of the device is in the range of 1060 to 1080 nm. First, an STL file for a cube part with dimensions of (8 × 8 × 8) mm<sup>3</sup> was created using Magics software from Materialise, Belgium. All cube parts were fabricated on a stainless steel substrate using various L-PBF process parameters. Using the Archimedes method to measure the density of these parts and calculate the relative density with 8.87 g/cm<sup>3</sup> as the theoretical (true) density, The theoretical (true) density of the Cu-0.3wt% CNTs composite powder was determined using a Multipycnometer<sup>TM</sup> (Quantachrome Instruments). In addition, all L-PBF experiments were conducted without preheating the build plate.

The printing employs a segmented scanning strategy, with each layer being 6mm in length, and the laser beam being rotated 67° per layer during scanning. Using the Archimedes method to measure the density of these parts and calculate the relative density, The theoretical (true) density of the Cu-0.3wt% CNTs composite powder was determined using a Multipycnometer<sup>TM</sup> (Quantachrome Instruments). relative density.

Select an optimized L-PBF setting that produces the highest part density (laser power 380W, scanning speed 230mm/s, scanning spacing 0.1mm), and the print parameters for both pure Cu material samples and Cu-CNTs composite samples are consistent. This parameter is used to make dog-bone samples for testing mechanical properties.

JEM-IT500 tungsten filament scanning electron microscope (SEM) from Japan Electronics was used to observe the microscopic morphology of the sample in greater detail. The X-ray diffractometer Bruker D8 ADVANCE made in Germany was used to detect the phase of the sample, and the scanning angle was 10° to 90°.

MDI JADE6.0 software was used to process and analyze the test data. The grain orientation and texture of the sample were analyzed by electron backscatter diffraction scanning (EBSD) using a JSM-7900F field emission scanning electron microscope from Nippon Electronics, and then the data were processed using Channel 5 software. In order to test its mechanical properties, dog-bone tensile specimens of 10502mm were printed according to GB/T 228.1-2010 standard, as shown in Fig.1a, and tensile tests were carried out at a

rate of 1mm/min on Instron M4206. Thermal conductivity is measured using a thermal conductivity meter (Hot

Disk2500s), and the size of the printed samples is 10\*10\*2mm, as shown in Fig.1b.

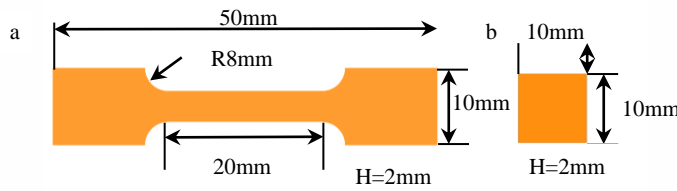


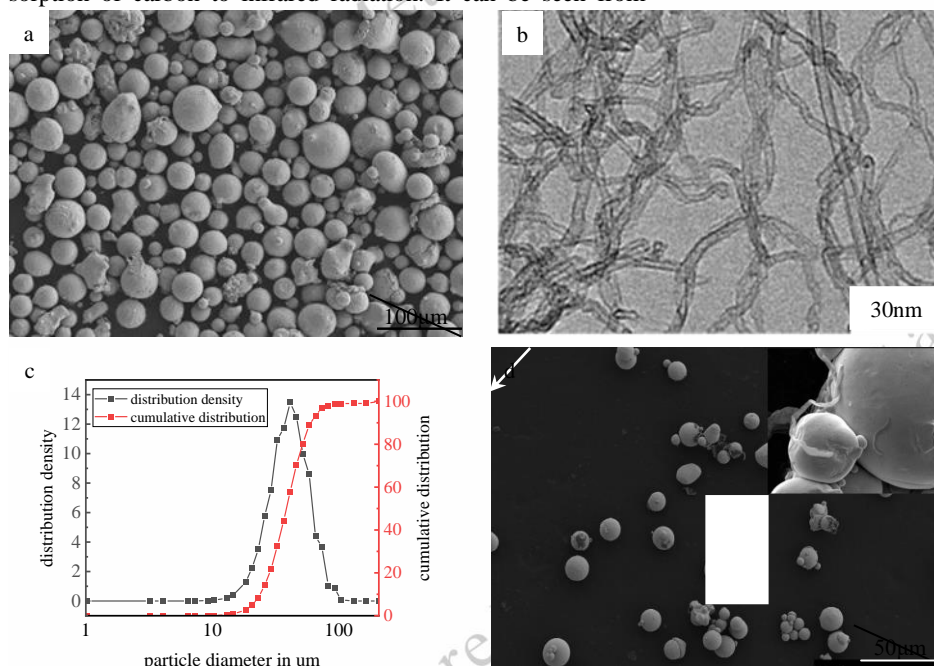
Fig.1 a tensile part sample and b thermal conductivity test sample

## 2 Results and Discussion

### 2.1 Formability

The particle size, microscopic morphology, laser absorptivity, and Raman spectrum results of the Cu-CNTs mixed powder are shown in Fig.2. As can be seen from the data in Fig.2a, the median particle size D50 of the mixed powder is 38.83 $\mu\text{m}$ , which fully satisfies the requirement for powder particle size (13-53 $\mu\text{m}$ ) for laser powder bed fusion technology. As can be seen from Fig.2b, the sphericity of the Cu powder is well maintained during the preparation of the mixed powder and is not compromised during the preparation process. The basic structure of CNTs dispersed by ultrasonic waves was not seriously damaged. As can be seen from Fig.2c, the light absorption rate of the Cu-CNTs mixed powder was 48.7% and that of pure Cu powder was 23.4% in the wavelength range of 1060-1080nm, and the light absorption rate of the Cu-CNTs mixed powder was 108.1% higher than that of pure Cu powder. It was found that the addition of CNTs significantly enhanced the light absorption rate of copper powder. This is attributed to the high optical absorption of carbon to infrared radiation. It can be seen from

Fig.2d that the Raman spectral characteristics of the mixed powder were not significantly altered compared to those of the original CNTs. The ID0/IG0 ratio of the original CNTs was 1.171, while the ID1/IG1 ratio of the water-bath ultrasonically homogenized carbon nanotubes was 1.208. The integrity of the water-bath ultrasonically homogenized CNTs was well maintained, being comparable to that of the original CNTs. The integrity of the water-bath ultrasonically homogenized CNTs decreased by 3.1% compared to the original CNTs, indicating that water-bath ultrasonic homogenization could better preserve the structural integrity of CNTs. The IG0/I2D0 ratio of the original CNTs was 2.581, and the IG1/I2D1 ratio of the ultrasonically homogeneous CNTs in water bath was 2.431. It was found that ultrasonic homogenization in water bath led to a reduction in the number of CNT layers, due to the forces exerted on CNTs during the homogenization process causing the separation of the layers. Compared to the original CNTs, the number of layers in the water-bath ultrasonically homogeneous CNTs increased by 6.2%, indicating that ultrasonically homogeneous CNTs could better maintain the integrity of CNTs.



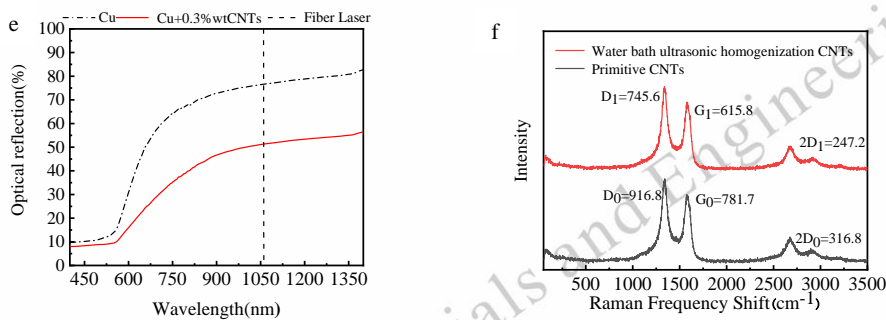


Fig.2 a shows the microscopic morphology of the initial CU powder, and b shows the microscopic morphology of the initial CNTs, c show the particle size of the CU-CNTs mixed powder; d shows the microscopic morphology of the CU-CNTs mixed powder; e shows the light (laser) absorption of the two powders (pure Cu and Cu + 0.3% wtCNTs) at different wavelengths from 400 nm to 1400 nm; f Shows Raman spectra of conventional CNTs and aquatic ultrasonic homogeneous CNTs

Cu-CNTs composites were successfully fabricated under the specified process parameters. The combination of process parameters included laser power of 380W, scanning speed of 230mm/s, scanning spacing of 0.1mm, and powder layer thickness of 0.03mm. The density of the Cu-CNTs composites was 96.6%. The density of the prepared Cu composites was 92.3%. The corresponding optical images are shown in Fig.3c and 3d. There are noticeable pores and a negligible amount of un melted powder in the pure Cu sample, as indicated by the black arrows. The presence of unmelted powder stems from the low laser absorption rate of pure Cu powder, leading to a significant amount

of energy being reflected and only a small portion being utilized for sample construction. Consequently, the powder between the two melt pools is less likely to melt, leading to an increase in defects. However, due to the incorporation of CNTs with a higher laser absorption rate, more energy was employed in constructing Cu-CNTs composite samples. This resulted in a significant reduction in surface defects and virtually no un melted powder. Consequently, with the inclusion of CNTs, the non-melting phenomenon of the powder vanished, and the number of pores was also reduced.

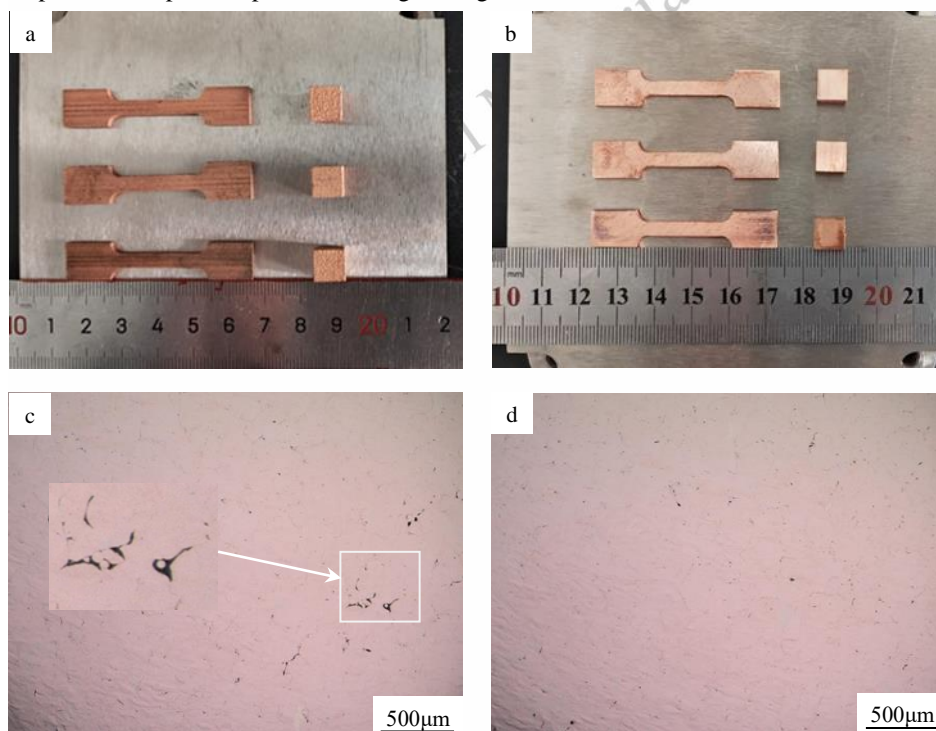


Fig. 3 a shows the macro morphology of the prepared pure copper sample, b shows the macro morphology of the prepared Cu-CNTs composite sample, c shows the defect diagram of the prepared pure copper sample, and d shows the defect diagram of the prepared Cu-CNTs composite sample

## 2.2 Microstructure

As observed in the XRD pattern in Fig.4 a, CNTs added to the pure copper material did not result in the formation of impurity phases with Cu during the manufacturing process. Meanwhile, a Raman spectrometer was used to test the prepared sample, and the spectrum is shown in Fig.5e. There is no characteristic peak of CNTs in the Raman spectrum of Cu samples, while there is an obvious G-band in Cu-CNTs composite sam-

ple. During LPBF, CNTs are surrounded by molten metal and covered by a solidified metal matrix, which may affect Raman scattering results. Therefore, the samples of Cu-CNTs composites showed a pronounced G-band peak. The G-band corresponds to the vibration of carbon-carbon bonds within CNTs, which confirms that carbon nanotubes are still present in the prepared composite samples.

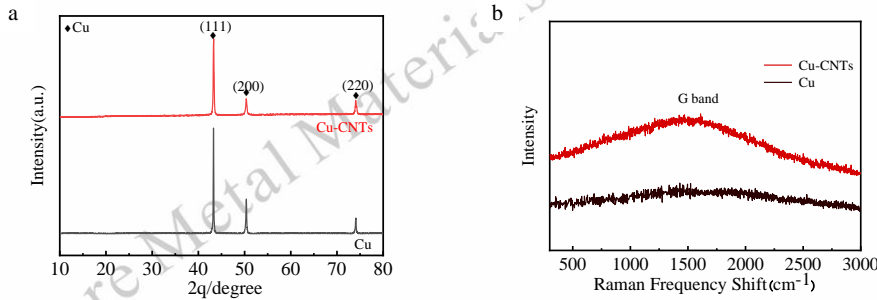


Fig.4 a shows the relative XRD intensity of Cu and Cu-CNTs composites, b shows the Raman spectrum detection of internal CNTs by Cu and Cu-CNTs composites

The grain morphology and size were analyzed through large-area EBSD analysis with a step size of 0.9  $\mu\text{m}$ , and the grain boundary angular orientation is depicted in Fig.5. In the IPF map depicted in Fig.5a-b, the regions of EG (equiaxed grain) and CG (columnar grain) are distinguishable. CG, or columnar grain, refers to the columnar grain region, whereas EG, or equiaxed grain, indicates the equiaxed grain region. According to the IPF map, the grain of the prepared sample exhibits no obvious preferred orientation. The CNTs content significantly influences the grain morphology of Cu material samples.

As illustrated in Fig.5a, columnar grains predominantly grow along the heat flow's negative direction (from the molten pool boundary to the molten pool center), while equiaxed grains are

randomly distributed along the molten pool boundary and within. However, upon adding CNTs to the Cu material, the grains started to differentiate into two categories in terms of shape and size: equiaxed grains (EG) at the edge of the molten pool and columnar coarse grains at the center of the molten pool, as indicated by the black arrow in Fig.5b.

As depicted in Fig.5a, equiaxed grains were initially randomly distributed within the Cu material sample. After incorporating CNTs into the Cu material sample, equiaxed grains started to accumulate near the molten pool's edge, leading to the formation of a greater number of larger columnar grains with similar orientations, which ultimately coalesced into larger columnar grains.

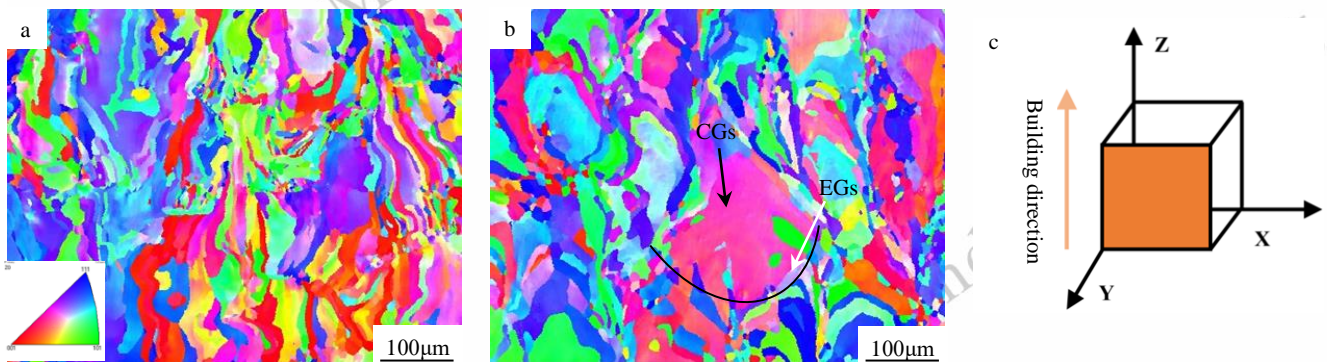


Fig.5 The IPF map obtained from EBSD with a step size of 0.9  $\mu\text{m}$  is shown in a, the Cu material sample is shown in b, the orange area in c is the test surface

The influence of CNTs on grain morphology might stem from their high thermal conductivity, which alters heat transfer dynamics within the molten pool. The impact of CNTs on the sample's microstructure is illustrated in Fig.6. The overall microstructure of the sample fabricated using LPBF is comparable to that of the pure Cu material sample, as depicted in Fig.6a. Owing to the well-oriented thermal gradient, which facilitates

epitaxial growth characteristic of LPBF, the grains within the molten pool are predominantly columnar, with a few equiaxed grains distributed relatively uniformly. However, for the composites, the EG at the boundary of the molten pool interfaces with the solidification zone, where heat dissipation is most rapid, leading to swift quenching; consequently, the grains typically manifest in the form of equiaxed equiaxed grains at the bound-

ary of the molten pool.

Drawing upon the nucleation sites supplied by CNTs, the elevated cooling rate of composites enhances the number of nucleation occurrences and the rate of heterogeneous nucleation<sup>[11]</sup>. A higher cooling rate results in a more rapid solidification rate, thereby constraining grain growth. The assimilation of laser energy, coupled with the swift solidification of the heterogeneous nucleation location, contributes to the development of equiaxed grains with a random orientation at the periphery of the molten pool<sup>[12]</sup>.

However, the grain size in the composite is observed to increase with the introduction of carbon nanotubes. This can be attributed to the fact that temperatures in the center of the molten pool exceed those at the edges, leading to overheating of the molten metal and the melting of some initial nucleation sites, thereby restricting nucleation rates and providing extended time for grain growth. This elucidates the disparity in grain morphologies observed between the center and the periphery of the molten pool.

Moreover, CNTs exert an influence on the alteration of heat transfer dynamics within composites. Typically, the heat flow direction in LPBF progresses from the center of the molten pool

towards the boundary, as succinctly indicated by a red arrow in Fig.6a. Incorporating CNTs can enhance heat transfer rates and temperature gradients, thereby facilitating the development and growth of columnar grains. Consequently, columnar grains sharing similar orientation amalgamate into larger, coarser columnar grains, as depicted in Fig.6b.

Regarding the Cu material sample, columnar grains develop in a direction opposite to that of the heat flow. Upon the addition of CNTs to the material, the thermal conductivity and cooling rate of the composite both escalated, rendering it easier for the edge of the molten pool to form equiaxed grains, whereas the center of the molten pool inclined towards the formation of columnar grains due to the well-aligned temperature gradient. Heat transfer is facilitated in proximity to the highly heat-conducting CNTs. Within the composite samples, carbon nanotubes constituted a larger portion of the heat transfer pathway in the molten pool, thereby promoting the formation of a greater number of longer, similarly oriented columnar grains. These grains amalgamate to form larger grains. Hence, incorporating CNTs led to the heterogeneous microstructure of the Cu-CNTs composites.

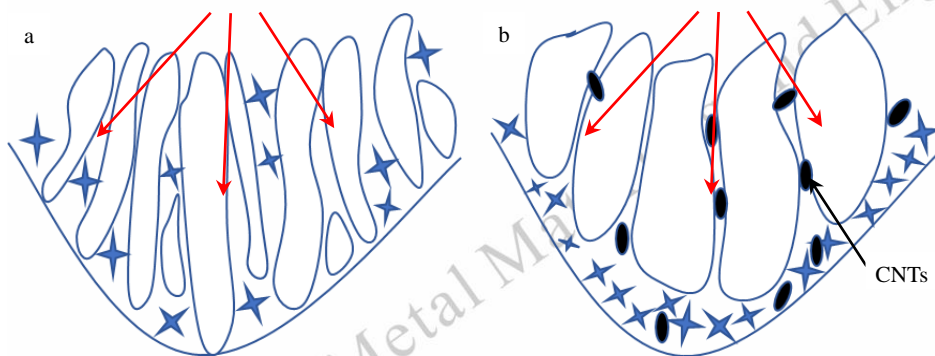


Figure 6: a schematic illustration depicting the impact of CNTs on the microstructure of specimens

CNTs also exerted a significant influence on the recrystallization structure distribution within the composites. As illustrated in fig.7 a and b, the deformed microstructure of Cu-CNTs material samples was notably more pronounced compared to that of pure Cu material samples. This is attributed to the fact that CNTs are nanoscale fibers. During the formation process, grains at the melt pool boundary interface with the solidification region, where heat dissipation is expedited and rapid quenching ensues, leading to equiaxed grain increase and the amplification of dislocation density among equiaxed grains. Consequently,

rendering recrystallization a challenging process. In summary, the enhancement of the deformed microstructure optimizes the material's mechanical properties, rendering it more capable of withstanding high loads and pressures. Moreover, the substructure generated within the grain will become more intricate, contributing to the enhancement of the material's overall properties. The augmented content of deformed tissue will elevate the dislocation density, accelerating the material's recovery rate in subsequent heat treatment processes to some extent, and aiding in the reduction of material processing time.

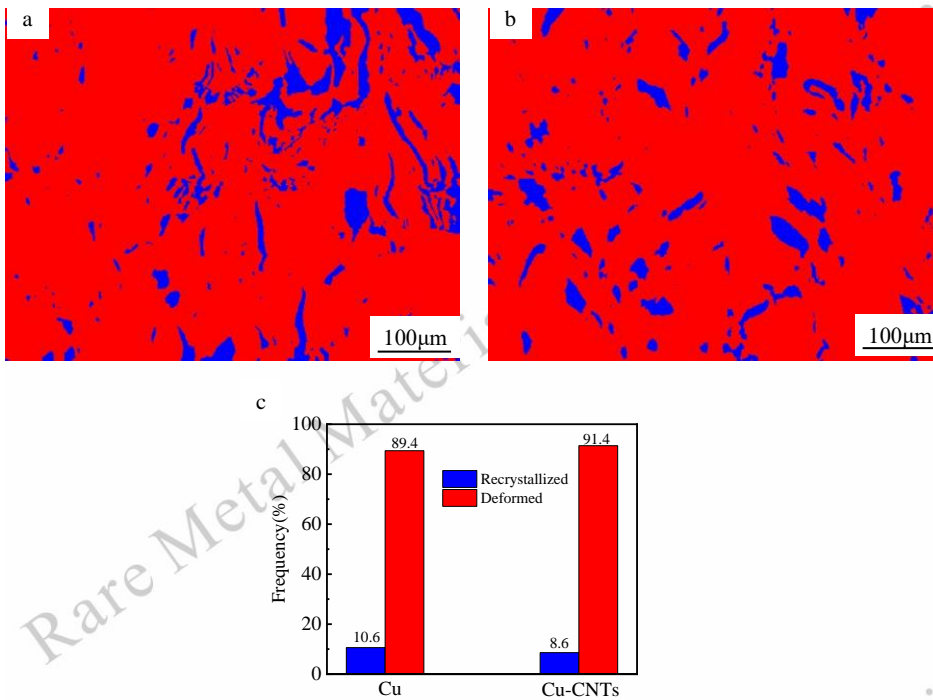


Fig.7 is the recrystallization diagram. a is the sample of Cu material, b is the sample of Cu-CNTs composite material, and c is the distribution of recrystallization and deformation

### 2.3 Mechanical property

It can be seen from the tensile data in Fig.8 that the tensile strength of the Cu material sample is 145.7 MPa and the elongation is 11.2%, while the tensile strength of the Cu-CNTs composite material sample is 222.6 MPa and the elongation is 27.6%. In contrast, the addition of CNTs increased the tensile strength of the composite by 52.8% and the elongation by

115.9%.

In the tensile curve shown in Figure 8, under the condition of minimal strain, the stress declines. This is because the two samples prepared are not fully dense, and there are micro-cracks, micro-holes and other defects in the samples, and local deformation occurs at the initial stage of loading, resulting in a slight decrease in stress.

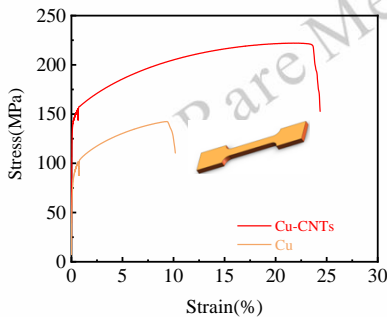


Fig.8 presents the comparison of the tensile properties between the Cu sample and the Cu-CNTs composite sample at room temperature

**Table 1 Tensile engineering stress-Strain curves**

	Stress (MPa)	Strain (%)
Cu	145.7	11.2
Cu/CNTs	222.6	27.6

The improvement of tensile properties of composites may be due to the following strengthening methods. Orowan strength-

ening and load transfer strengthening are strongly dependent on the volume fraction of CNTs. The main strengthening mecha-

nism of composites with a high carbon nanotube aspect ratio is load transfer<sup>[13,14]</sup>. CNTs are present in composites, suggesting that Orowan strengthening may have a significant strengthening effect on Cu-CNTs composites.

Grain boundary strengthening is closely related to the average grain size, also known as Hall-Petch strengthening. However, according to the EBSD grain information in Fig.5, the aver-

age grain size of the Cu-CNTs material sample was relatively larger. Therefore, grain boundary strengthening may not be one of the main strengthening mechanisms. In addition, the addition of CNTs and the heterogeneous structure induced by CNTs formed a mechanism of back stress strengthening during the deformation of Cu-CNTs composites, which improved the strength and plasticity of the materials<sup>[15-17]</sup>.

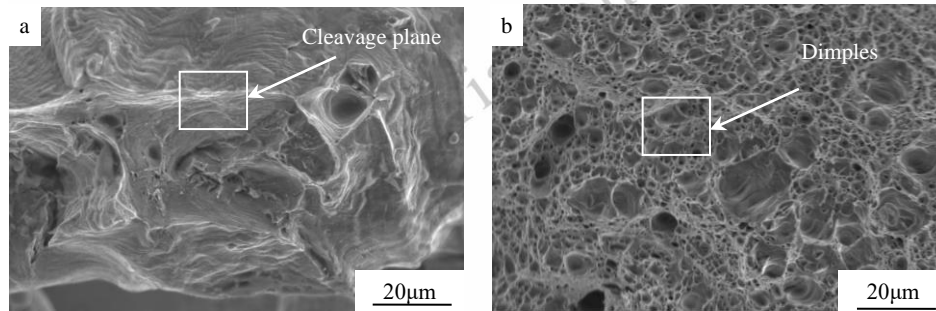


Fig.9 a show the fracture morphology of the tensile portion of the Cu sample, b shows the fracture morphology of the tensile portion of the Cu-CNTs composite sample

The fracture morphology of CNTs/Cu composites prepared by the L-PBF method is shown in Fig.9 b, and CNTs have a significant influence on the fracture morphology of samples. It can be seen from Fig.9 a that the fracture morphology of the tensile part of the Cu material sample shows a large number of cleavage planes and only a small number of dimples. The low elongation of the sample is attributed to quasi-cleavage fracture and the presence of large defects. It can be seen from Fig.9 b that the fracture morphology of the tensile parts of Cu-CNTs composites after tensile fracture is characterized by a large number of dimples, with the dimples appearing as small dimples within the large dimples. It can be demonstrated that the tensile properties and elongation of Cu-CNTs composites are significantly improved compared with Cu materials. This is because the addition of CNTs increases the material's energy absorption rate, with more energy utilized to melt the metal powder, resulting in a reduction in the number of defects and pores within the material. Therefore, during the stretching process, dislocations accumulate at the grain boundaries, leading to stress concentration that causes the interface to debond and form a tiny cavity. The material between the cavities is stretched, resembling a jut. The cavities connect to form dimples, which makes the composite material less prone to breaking. However, the defects in Cu material samples are relatively larger. When

stress concentration occurs due to the accumulation of dislocations at the grain boundaries during the stretching process, micro-cracks tend to form at these defects, and the cracks propagate rapidly and directly, making it easier for the material to fracture.

#### 2.4 Thermal conductivity

The table 2 summarizes the thermal conductivity of the finished L-PBF parts processed by carbon nanotubes mixed with copper powder, and compares it with the performance of the Cu material sample. In comparison, the thermal conductivity of the Cu-CNTs composite sample is higher. Compared with the Cu material sample, the thermal conductivity of the Cu-CNTs composite sample increased from 405.54 W/(m\*K) to 449.34 W/(m\*K), an increase of 10.8%. Thermal diffusion increased from 120.96 mm<sup>2</sup>/s to 134.97 mm<sup>2</sup>/s, an increase of 11.6%. The specific heat capacity decreased from 0.41 J/g/K to 0.39 J/g/K, a reduction of 4.8%. Using Wiedemann-Franz's law, the electrical conductivity of parts can be calculated theoretically. Considering the Lorentz constant (L) = 2.44 × 10<sup>-8</sup> WΩ/K<sup>2</sup> [18] and temperature T = 300 K, the calculated conductivity is 617.76 × 10<sup>6</sup> S/m. Compared with the composite material, the electrical conductivity of pure copper sample is increased from 5.5 × 10<sup>7</sup> S/m to 6.2 × 10<sup>7</sup> S/m, and the electrical conductivity is increased by 12.7%.

**Table 2 shows the heat transfer rate, thermal conductivity, specific heat capacity, and electrical conductivity of the sample Cu material and the sample Cu-CNTs composite material**

	Thermal diffusivity (mm <sup>2</sup> /s)	thermal conductivity (W/(m*K))	specific heat (J/g/K)	electric conductivity (S/m)
Cu	120.96±0.06	405.54±0.20	0.41±0.01	5.5 × 10 <sup>7</sup>
Cu/CNTs	134.97±0.89	449.34±2.97	0.39±0.01	6.2 × 10 <sup>7</sup>

CNTs, due to their nanostructure and high aspect ratio, provide highly efficient paths for the transport of phonons and electrons. Their carbon-carbon bonding endows the material

with excellent thermal and electrochemical stability, resulting in extremely high thermal and electrical conductivity<sup>[19]</sup>. When CNTs are added to copper matrix materials, they maintain high

thermal and electrical conductivity. Dispersed CNTs partially replaced the copper thermal conductivity network in the copper matrix, constructing a new network with enhanced thermal conductivity. Compared to the thermal conductivity of the copper matrix material, the new thermal conductivity network exhibits superior phonon and electron transport capacity. The addition of CNTs significantly enhanced the thermal conductivity of the Cu material.

### 3. Conclusions

In this study, CNTs-Cu composites were prepared by the LPBF method. The formability, microstructure, mechanical properties, and electrical and thermal conductivity of CNTs-Cu composites were studied. The main conclusions are as follows:

1) Ultrasonic homogenization in water minimized structural loss of CNTs, and CNTs improved the laser absorption rate of composites. Under the optimal parameter combination, CNTs-Cu composites were successfully prepared by the LPBF method, and the sample density of the prepared materials reached 96.6%.

2) CNTs, due to their high thermal conductivity, can alter the heat transfer behavior and cooling rate of the composite material. CNTs also modify the local temperature gradient, resulting in the presence of equiaxial EG at the edge of the molten pool and CG heterogeneous structures in the center of the molten pool.

3) The tensile strength of the prepared CNTs-Cu sample reached 222.6 MPa at room temperature, and the elongation reached 25.95%.

4) The thermal conductivity of the prepared CNTs-Cu composite reached 449.34 W/(m·K), and the electrical conductivity reached 99.66% IACS.

### References

- 1 Yap C.Y, Chua C.K., Dong Z.L et al. *Applied Physics Review*[J] 2015,2,041101
- 2 Reimund Neugebauer, Bernhard Müller, Mathias Gebauer et al. *Assembly Automation*[J]2011,31,344-347
- 3 Thang Q. Tran, Amutha Chinnappan, Jeremy Kong Yoong Lee et al. *Metals* [J]2019,9,756
- 4 Shasha Zhang, Haihong Zhu, Luo Zhang et al. *Materials Letters*[J]2019,237,306-309
- 5 Christopher Walli, Bruno Buchmayr. *Materials Science Engineering: A* [J]2019,744,215-223
- 6 Matías Sabelle, Magdalena Walczak, Jorge Ramos-Grez. *Optics and Lasers in Engineering*[J]2018,100,1-8.
- 7 Shasha Zhang, Haihong Zhu, Zhiheng Hu et al. *Powder Technology*[J]2019,342,613-620
- 8 Suraj Dinkar Jadhav, Jozef Vleugels, Jean-Pierre Kruth et al. *Material Design & Processing Communications*[J]2019, 7,15
- 9 Riccardo Casati, Maurizio Vedani. *Metals* [J]2014,4 ,65-83
- 10 Suraj Dinkar Jadhav, Sasan Dadbakhsh, Jozef Vleugels et al. *Materials*[J]2019,12,2469
- 11 Arvind Prasad, Lang Yuan, Peter Lee et al. *Acta Materialia*[J]2020,195,392-403
- 12 Mohammad Reza Jandaghi, Hesam Pouraliakbar, Vahid Fallah et al. *Materials Characterization*[J]2022,192, 112206
- 13 Jong Gil Park, Dong Hoon Keum, Young Hee Lee. *Carbon*[J]2015,95,690-698
- 14 Z.Y. Liu, B.L. Xiao, W.G. Wang et al. *Carbon* [J]2012,50 ,1843-1852
- 15 Y. Morris Wang, Thomas Voisin, Joseph T. McKeown et al. *Nature Materials*[J]2018,17 ,63-71,
- 16 Run Xu, Genlian Fan, Zhanqiu Tan et al. *Materials Research Letters*[J]2018, 6 ,113-120
- 17 Zihong Wang, Xin Lin, Nan Kang et al. *Additive Manufacturing* [J]2020,34, 101260
- 18 Sebastian J. Raab, Ralf GuschlbauerLodes, Matthias A. Lodes et al. *Advanced Engineering Materials* [J]2016,18,1661-166
- 19 Valentin N. Popov. *Materials Science and Engineering R* [J]2004, 43,61-102

## CNTs 的添加对激光粉末床熔融纯铜的微观结构和力学及导电导热性能的影响

杨来侠<sup>1</sup>, 张龙博<sup>1</sup>, 谢启东<sup>2</sup>, 张晏泽<sup>1</sup>, 杨蒙佳<sup>1</sup>, 毛峰<sup>3</sup>, 陈祯<sup>2</sup>

(1. 西安科技大学 机械工程学院, 陕西 西安 710054)

(2. 西安交通大学 机械工程学院, 陕西 西安 710049)

(3. 龙门实验室, 河南 洛阳 471000)

**摘要：**激光粉末床熔合（L-PBF）工艺制造铜通常表现出较差的强度-塑性配合，添加增强相通常是改善这种配合的有效方法。然而，对 Cu 复合材料的研究相对有限。为了探究增强相对 Cu 的影响，我们以 Cu-CNTs 混合粉末为基体，采用 L-PBF 技术制备 Cu-CNTs 复合材料。研究了其成形性能、微观结构、力学性能、导电性能和热性能。所得复合材料具有较高的的相对密度。CNTs 的加入导致了熔池边缘等轴晶粒和中心柱状晶粒的不均匀组织。与纯铜相比，复合材料的整体力学性能得到改善（抗拉强度提高 52.8%，伸长率提高 115.9%），电性能和热性能也得到提高（导热系数提高 10.8%，电导率提高 2.5%）。结果表明，CNTs 的加入可以提高铜的抗拉强度和伸长率，以及铜的电学和热学性能。因此，这种材料为设计更高效的散热器结构提供了有效途径。

**关键词：**激光粉末床熔融；Cu-CNTs 复合材料；力学性能；热导率

作者简介：杨来侠，女，1961 年生，博士，教授，西安科技大学机械工程学院，陕西 西安 710054，E-mail: [yanglx@xust.edu.cn](mailto:yanglx@xust.edu.cn)